ACS APPLIED MATERIALS & INTERFACES

Research Article

www.acsami.org

# Photosensitivity Enhancement with $TiO_2$ in Semitransparent Light-Sensitive Skins of Nanocrystal Monolayers

Shahab Akhavan,[†] Aydan Yeltik,[†] and Hilmi Volkan Demir*[,†,‡]

[†]UNAM—Institute of Materials Science and Nanotechnology, Department of Electrical and Electronics Engineering, and Department of Physics, Bilkent University, Ankara, 06800, Turkey

[‡]School of Electrical and Electronic Engineering and School of Physical and Mathematical Sciences, Nanyang Technological University, Singapore, 639798, Singapore

Supporting Information

**ABSTRACT:** We propose and demonstrate light-sensitive nanocrystal skins that exhibit broadband sensitivity enhancement based on electron transfer to a thin $TiO_2$ film grown by atomic layer deposition. In these photosensors, which operate with no external bias, photogenerated electrons remain trapped inside the nanocrystals. These electrons generally recombine with the photogenerated holes that accumulate at the top interfacing contact, which leads to lower photovoltage buildup. Because favorable conduction band offset aids in transferring photoelectrons from CdTe nanocrystals to the $TiO_2$ layer, which decreases the exciton recombination probability, $TiO_2$ has been utilized as the electron-accepting material in these light-sensitive nanocrystal skins. A controlled interface thickness between the $TiO_2$ layer and the monolayer of CdTe nanocrystals enables a photovoltage buildup enhancement in the proposed nanostructure platform. With $TiO_2$ serving as the electron acceptor, we observed broadband sensitivity improvement across 350−475 nm, with an approximately 22% enhancement. Furthermore, time-resolved fluorescence measurements verified the electron transfer from the CdTe nanocrystals to the $TiO_2$ layer in light-sensitive skins. These results could pave the way for engineering nanocrystal-based light-sensing platforms, such as smart transparent windows, light-sensitive walls, and large-area optical detection systems.

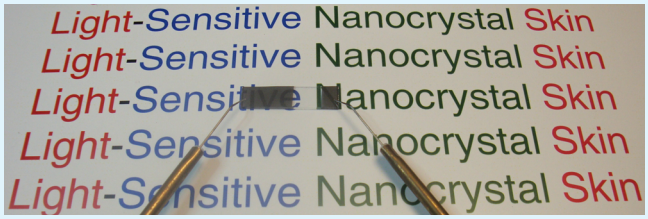


**KEYWORDS:** *semiconductor quantum dots, nanocrystals, $TiO_2$, light-sensing, voltage buildup, self-assembled monolayers, time-resolved fluorescence*

Semiconductor nanocrystals (NCs)[1−3] are currently used to create novel optoelectronic devices for the photovoltaic,[4−6] light-emission,[7−9] light-detection,[10,11] and biosensing[12,13] applications. Solution-processable NCs, which have been developed for over the past two decades,[14] have been heavily exploited in optoelectronic applications, and emerging usage fields of these intriguing materials are still developed for novel devices.[15] From the material perspective, NCs offer a number of useful attributes: (1) they are low cost; (2) they are solution processable; (3) they have spectral tunability due to the quantum size effect, and (4) they can easily be deposited on a variety of substrates.

NC-based photodetectors convert an optical signal to an electrical signal using the NCs as the optical absorbers.[16,17] They are easy to fabricate at low cost, which makes them good candidates for large-area light-sensing applications. These devices were initially constructed on the basis of charge collection, where an electric field imposed on the photodetector dissociates the photogenerated excitons into electrons and holes, and an electric current is produced.[18] Recently, another device structure called the light-sensitive nanocrystal skin (LS-NS) has been developed.[19] Unlike the charge collection mechanism, they are operated on the principle of photogenerated potential buildup. Their ability to provide reliable data that has high sensitivity at the required wavelength, high conversion efficiency of photons to an electrical signal, low noise that results in a high signal-to-noise ratio, along with the possibility to make them over large areas offers a promising approach for the light-sensing applications.

LS-NSs consist of a monolayer of NCs over the polyelectrolyte polymers on top of a thin stack of high-dielectric spacing layers made of hafnium dioxide ($HfO_2$). These devices operate on the basis of photogenerated potential buildup with the aid of $HfO_2$ as the charge isolation layer on top of the indium tin oxide (ITO) contact, and the interaction between the NCs and the top interfacing contact. Despite the single NC layer in LS-NSs, they are highly sensitive devices creating very low charge accumulation to achieve a large enough photovoltage buildup. Furthermore, a monolayer of NCs is advantageous to be used in LS-NSs owing to the properties of semitransperency, low material consumption, and low noise generation.

In LS-NSs, after the excitons are photogenerated, they are dissociated at the interface between the aluminum (Al) and the

Received: December 13, 2013
Accepted: May 12, 2014
Published: May 12, 2014

   dx.doi.org/10.1021/am502472y | ACS Appl. Mater. Interfaces 2014, 6, 9023−9028

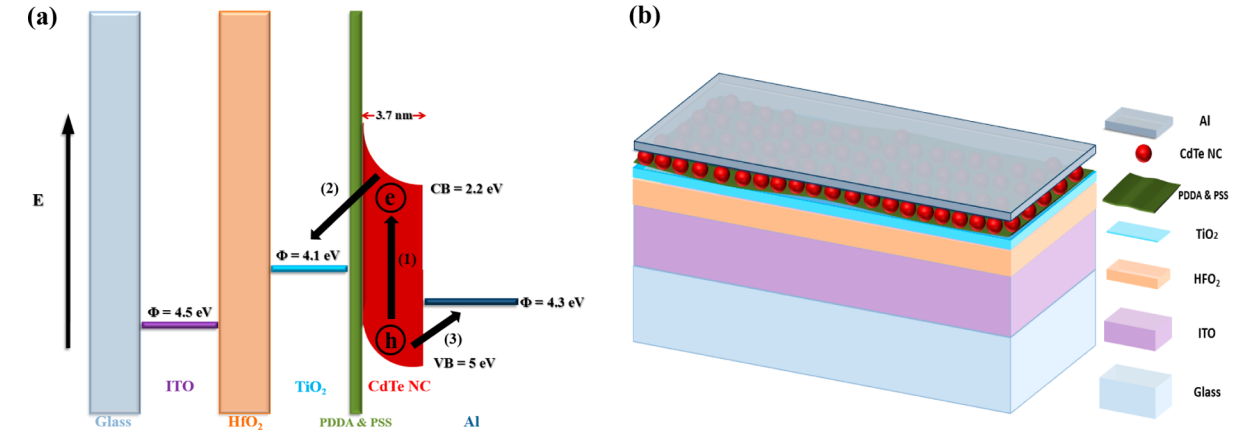


**Figure 1.** (a) Energy band diagram of CdTe NC (3.7 nm in size) conduction band (CB), valence band (VB), and the workfunction (Φ) of ITO, $TiO_2$, and Al are shown in the energy diagram. After the excitons are photogenerated (1), electrons are transferred to the $TiO_2$ layer (2), while holes migrate to the Al side (3). (b) Schematic of the LS-NS device incorporating a $TiO_2$ layer.

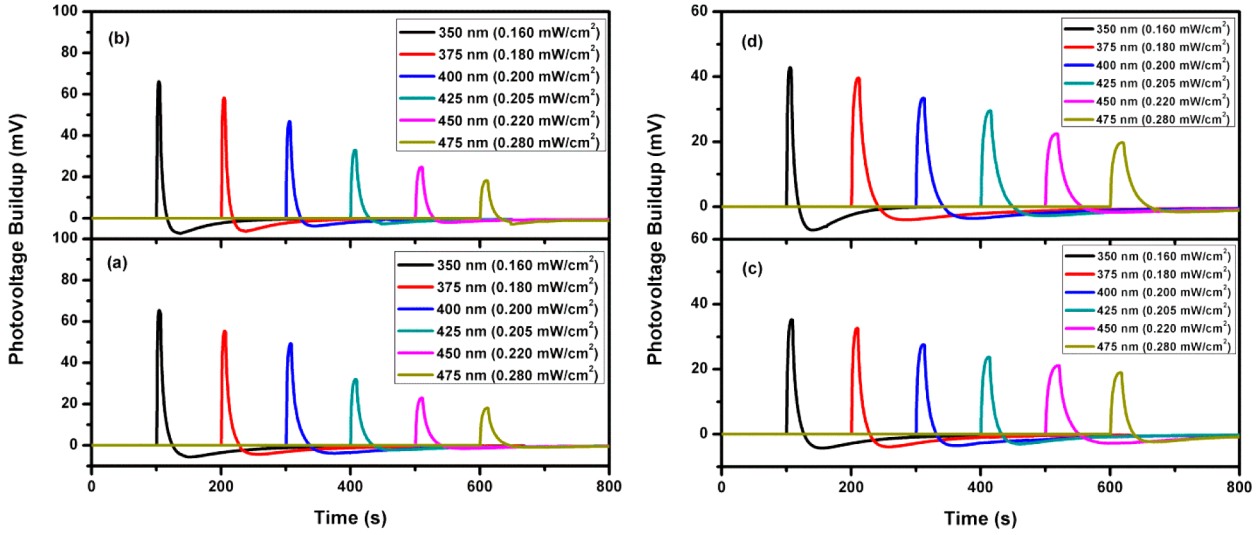


**Figure 2.** Variations of the photovoltage buildup based on four bilayers of PDDA−PSS at different excitation wavelengths (a) without $TiO_2$ and (b) with $TiO_2$. Photovoltage buildup variation based on one bilayer of PDDA−PSS (c) without $TiO_2$ and (d) with $TiO_2$.

NC monolayer. Owing to the Al workfunction and band alignment of the NC monolayer, the holes migrate to the Al side, whereas the electrons remain inside the NCs due to the presence of the $HfO_2$ layer. In these devices, the more electrons and holes that are photogenerated, the more voltage buildup that can be obtained. These electrons and holes tend to recombine inside the NCs; therefore, the competition between exciton dissociation and recombination affects the performance in a negative way. Consequently, we posit that, by transferring electrons from the NCs to an electron acceptor layer, and thus further separating the holes and electrons to decrease the recombination probability, a favorable enhancement in the device performance can be obtained. The higher conduction band level of NCs can serve as the driving force for electron injection from the NCs to a nearby acceptor with a lower conduction band level. To this end, we propose that a favorable conduction band offset in LS-NS devices may aid in transferring electrons from the NCs to an electron-accepting material such as $TiO_2$. Hence, the majority of holes migrate toward the top Al contact. A schematic band diagram of the $TiO_2$ and Al, which serve as the acceptors for the electrons and the holes, respectively, is shown in Figure 1a.[20] The device architecture for the light-sensitive skins with the electron-accepting layer ($TiO_2$) is also depicted in Figure 1b.

We fabricated light-sensitive skins both with the $TiO_2$ layer (w $TiO_2$) and without the $TiO_2$ layer (wo $TiO_2$) to be used as a reference sample. In the quest to find a proper electron-accepting material, Jin et al. reported the process of charge transfer from NCs to a $TiO_2$ layer grown by atomic layer deposition (ALD).[21] This process uses pulses of water that preferentially coat hydrophilic surfaces and improve the quality of self-assembled films.[22] An absorption spectrum of the 10 nm thick $TiO_2$ film via ALD is given in the spectral range of 350−600 nm (see Figure S1, Supporting Information).

We also synthesized aqueous CdTe NCs of different sizes according to the study reported by Rogach et al.[23] Different LS-NS devices were fabricated based on these NCs with the average diameters of 2.9 and 3.7 nm, which is found from their extinction spectra[24] (Figure S2, Supporting Information). To enhance electron transport and charge conductivity, we partially removed the thioglycolic acid (TGA) ligands from the NC surfaces by adding isopropanol into the CdTe NC solution and centrifuging the mixture. We note that another means of decreasing the recombination probability of photogenerated


dx.doi.org/10.1021/am502472y | ACS Appl. Mater. Interfaces 2014, 6, 9023−9028

electrons and holes in these devices relies on surface passivation of the NCs.[1] Indeed, charges encounter high potential barriers due to the ligands passivating the NCs' surface. During the film assembly, the NC solution was rigorously stirred to prevent precipitation. Ligand removal of CdTe NCs and monolayer assembly procedures are all explained in our previous work in detail.[25]

For the device implementation, after cleaning the indium tin oxide (ITO) film deposited on a glass substrate, a 50 nm thick $HfO_2$ dielectric film, followed by a 10 nm $TiO_2$ layer, was deposited using ALD at 150 °C. Subsequently, we used layer-by-layer assembly[26] via a computerized dip-coating system to deposit the NCs. Negatively charged CdTe NCs were coated on top of bilayers of polydiallyldimethylammonium chloride–polysodium 4-styrenesulfonate (PDDA–PSS) serving as a strong polyelectrolyte polymer layer. Finally, a very thin semitransparent Al contact was deposited on top of the NC layer using a thermal evaporator (Figure 1b).

## RESULTS AND DISCUSSION

For a detailed understanding of the effects of $TiO_2$ layer incorporation into the light-sensitive skins in terms of the device operation and performance, we systematically changed the excitation wavelength and the illumination intensity. The photovoltage buildup vs time characteristics for the devices (wo/w $TiO_2$) with four bilayers of PDDA–PSS obtained under a monochromatic light source is shown in Figure 2a,b. We observed more voltage buildup as the excitation wavelength is shortened, followed by a larger negative voltage value after the light was switched off. This result is due to the stronger optical absorption of CdTe NCs at shorter optical wavelengths. At higher photon energies, due to the more available electron and hole states, NCs can absorb a larger number of photons and photogenerate more electron–hole pairs. On the other hand, the lower voltage buildup observed in the low photon energy region is owing to the low optical absorption of the NCs, which is a limiting factor for the device performance.[27] The devices wo/w $TiO_2$ based on the four bilayers of PDDA–PSS showed similar voltage buildup variations in response to the excitation with different intensities at different wavelengths. We did not observe any considerable improvement in the output of the device w $TiO_2$ as compared to that of the device wo $TiO_2$. This implies that the $TiO_2$ layer did not significantly affect the charge-transfer mechanism when the four-bilayer PDDA–PSS is used in the device. In these structures, electrons were, therefore, not able to migrate sufficiently to the $TiO_2$ layer.

As depicted in Figure 1a, the conduction band edge of a CdTe NC lies above that of $TiO_2$ film, which favors the strong electron injection into the $TiO_2$ layer. To understand the underlying mechanism responsible for hindering the electron transfer to the $TiO_2$, we suggest that it might be the polyelectrolyte polymer thickness in our device structure. Therefore, we attribute the unvaried voltage buildup for the sample with the $TiO_2$ layer to the thickness of the polyelectrolyte polymer layer. When the polymer layer is thick enough to prevent the electron transfer to the $TiO_2$ layer, electrons are trapped inside the NCs and may recombine with the photogenerated holes at the interface between the NC and the Al layer. As a result, a similar amount of voltage buildup as in the case of the reference can be observed. Furthermore, when we used the generic definition of sensitivity as the ratio of voltage buildup to the incident optical power, again, no considerable change was observed, as seen from Figure 3a.

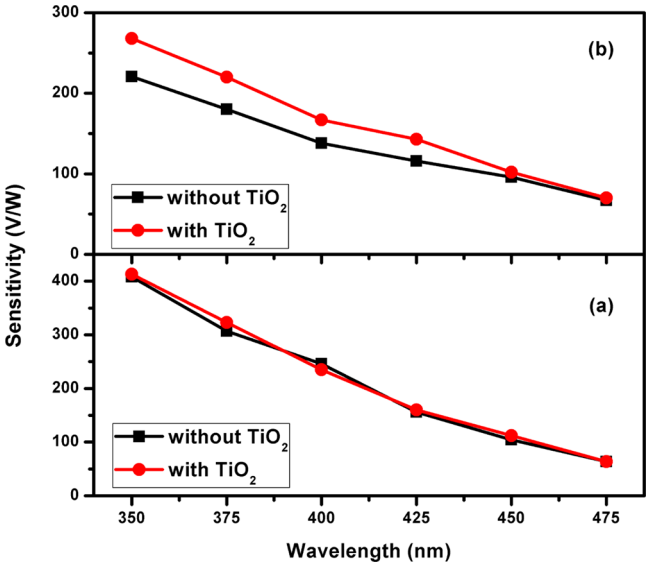


**Figure 3.** Sensitivity comparison of the LS-NS devices in the absence and presence of a $TiO_2$ layer for the structures, based on (a) four bilayers of PDDA–PSS and (b) one bilayer of PDDA–PSS.

If the dielectric polyelectrolyte layer is thin enough, the electrons will not be trapped inside the NCs and they will be transferred to the $TiO_2$. Consequently, the recombination probability of photogenerated excitons inside the NCs may decrease, which results in a larger photovoltage buildup. To this end, we decreased the number of polymer layers from four to one, to eliminate the possible change in the surface of the NCs as the number of polyelectrolyte layers changes,[28−30] and we fabricated an individual control sample for each set of samples. As shown in Figure 2c,d, the enhancement in electron injection into the $TiO_2$ layer was confirmed by the great increase in photovoltage buildup. In the presence of a thin polyelectrolyte polymer between the NCs and the $TiO_2$, electron transfer to the $TiO_2$ film takes place easily, which, in turn, decreases the recombination probability of the photogenerated electrons and holes in the NCs. This leads to a larger voltage buildup, which, consequently, enhances the device sensitivity. As can be understood from Figure 3b, we obtained a sensitivity enhancement over the broad spectral range of 350–475 nm with an increase of up to 22% when compared to the reference sample.

Furthermore, the sensitivity enhancement at the long wavelength region is less than that at the short wavelength region. In our previous work, we reported that the sensitivity of a NC skin increases with the plasmonic enhancement of the NC absorption by using plasmonic nanocrystals. The sensitivity improvement in plasmonically coupled light-sensitive skins of NC monolayers strongly depends on the localized plasmonic resonance band. That is why we posit that the enhancement is most likely only because of the charge-transfer mechanism and there is no absorption enhancement of the CdTe NC monolayer.[31] The slight enhancement in the performance of the both devices w/wo $TiO_2$ film at longer wavelengths can be attributed to the lower photon energies. These low-energy electrons and holes are less likely to cross the potential barrier of NCs and more likely to be captured at the surface states. This was also confirmed with the in-film photoluminescence excitation (PLE) and absorption data of the monolayer CdTe NCs (Figure S3, Supporting Information). To further verify the

excitation wavelength dependence of the device sensitivity, we conducted the voltage buildup measurements at different excitation wavelengths and intensity levels by using another LS-NS device with different-sized CdTe NCs. To this end, we used CdTe NCs with the diameter of 2.9 nm, having the first excitonic peak at around 530 nm, and fabricated LS-NS based on one bilayer of PDDA−PSS in the absence and presence of the $TiO_2$ layer (Figure S4, Supporting Information). Lower voltage buildup and correspondingly reduced sensitivity in the device performance can be explained by the lower optical absorption of the smaller NCs (2.9 nm in diameter). This is an expected result since the smaller (larger) NCs have a smaller (larger) number of states available due to the quantum confinement effects and the resultant lower (higher) optical absorption, which results in a lower (higher) voltage buildup. Moreover, small-sized NCs have generally a larger number of trap states than large-sized NCs, which limits the photogenerated exciton population. Consequently, as compared to the devices with the small NCs, better device performance was observed for the range of 350−475 nm by using the larger NCs, which has the first excitonic peak at around 605 nm and the photoluminescence emission peak at around 627 nm (Figure S5, Supporting Information). As an evidence for the effect of introducing the $TiO_2$ layer, there is a clear difference between the sensitivity enhancement levels at short and long wavelength ranges. In both devices w/wo $TiO_2$, photogenerated electrons and holes remain inside the NCs due to the lower photon energies at longer wavelengths. As a result, a lower voltage buildup and slight sensitivity enhancement can be observed in the long wavelength range.

To further support the existence of a charge transfer from the NCs to the $TiO_2$ film, we conducted time-correlated single-photon counting experiments (Picoquant, Fluotime 200) for a hybrid structure composed of the NC monolayer on top of the polymer layer and coated on 10 nm $TiO_2$, which is deposited on glass substrates and on the same structure, but without $TiO_2$. We prepared the samples by using a self-assembly technique via dip-coating and subjected the structures (wo/w $TiO_2$) to time-resolved fluorescence (TRF) spectroscopy at room temperature. The TRF system has a pulsed laser diode with an excitation wavelength of 375 nm and a calibrated time resolution of 32 ps. Time-resolved fluorescence detection was performed at the NC film's peak emission wavelength, which is 640 nm (Figure S6, Supporting Information). Figure 4 depicts the TRF decay curves for all the samples (wo/w $TiO_2$), and all the decay curves were analyzed by 1/e fitting. As evident from Figure 4, there is a clear difference between the TRF decays of the bilayered PDDA−PSS-based structures wo/w the $TiO_2$ layer. According to the measurement, the effective lifetime decreases considerably, from 0.796 ns in the sample with no $TiO_2$ to 0.467 ns in the sample with $TiO_2$. This reduction in lifetime supports the presence of a possible electron-transfer channel from the donor NCs into the acceptor $TiO_2$. Here, it is worth noting that, due to the lack of overlap between the $TiO_2$ absorption and the NC emission, we ruled out an energy transfer from the NCs to the $TiO_2$.[32,33]

Similarly, to verify the device demonstration in which the thick polyelectrolyte layers (the four bilayers of PDDA−PSS) limit the electron transfer from the NCs to the $TiO_2$ layer, we took the TRF measurements of the structures with a monolayer of CdTe NCs using four bilayers of PDDA−PSS wo/w the $TiO_2$ layer. The lifetimes of the structures based on four bilayers of PDDA−PSS in the samples wo/w $TiO_2$ were found

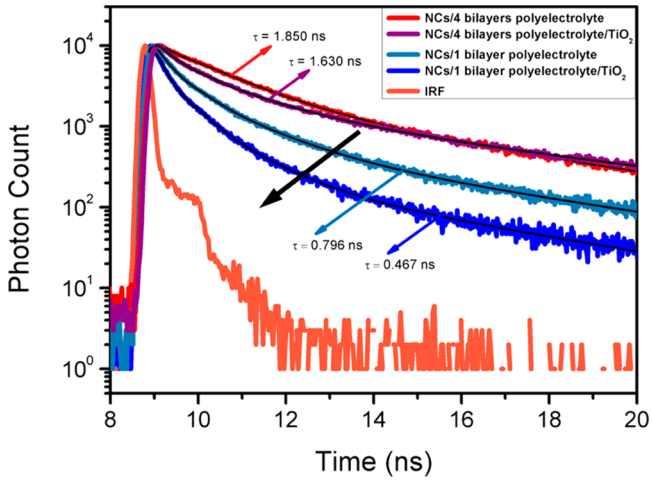


**Figure 4.** Time-resolved fluorescence decays of the NCs in the absence and presence of the $TiO_2$ layer based on different bilayers of polyelectrolyte polymers. The black arrow indicates the decrease in the lifetime of the NC samples based on one bilayer of polyelectrolyte polymers from the structure without the $TiO_2$ to the one with the $TiO_2$ layer. The electron-transfer rate of the one-bilayer case was found to be 0.89 $ns^{-1}$, whereas it is almost zero for the four-bilayer structure.

to be similar to each other, which are 1.850 and 1.630 ns for the samples wo/w $TiO_2$, respectively. The thick polyelectrolyte polymer layer must, therefore, hinder the migration of electrons to the $TiO_2$ film, which explains the aforementioned observation of no considerable performance improvement in the device operation.

To further analyze the lifetimes, we predicted the electron-transfer rate of the presented structures using the expression $\gamma_e = \gamma_{hybrid} - \gamma_{ref}$,[34,35] where $\gamma_{hybrid}$ is the rate for the monolayer NCs on top of the bilayers of polyelectrolyte polymers with the presence of $TiO_2$, and $\gamma_{ref}$ is the NCs' excited-state relaxation rate obtained from the structure with no $TiO_2$. By subtracting the rate of the hybrid structure from that of the reference for the one-bilayer-based PDDA−PSS, assuming that the difference can be attributed to the electron-transfer rate, we calculated a transfer rate of $\gamma_e = 0.89$ $ns^{-1}$. However, this rate is almost zero for the four-bilayer case. We also calculated the electron-transfer efficiency using the relation $\eta = \gamma_e/(\gamma_e + \gamma_{ref})$ and found the resulting efficiency for the one-bilayer case to be 41.3% which is a quite high value as compared to 11.9% obtained for the four-bilayer case. This significant efficiency explains the migration of a considerable amount of photogenerated electrons from the CdTe NCs to the $TiO_2$ layer. These observations are in strong agreement with the observed photovoltage buildup and sensitivity spectrum of the LS-NS with the $TiO_2$.

## CONCLUSION

In this paper, we demonstrated the transportation of photogenerated electrons to a $TiO_2$ layer in LS-NS devices leading to great enhancement in the device sensitivity. We observed that, depending on the thickness of the associated polyelectrolyte polymer layer, the sensitivity of the photosensors with the $TiO_2$ layer can be enhanced or remain unaffected. We verified that thick polyelectrolyte polymer layers serve as an unfavorable injection barrier for transferring photogenerated electrons to the $TiO_2$ layer. Subsequently, we designed our optimum

structure based on one bilayer of PDDA−PSS to improve the charge separation at the CdTe/$TiO_2$ interface, i.e., with the least amount of electrons being scarified. The measured photovoltage buildup spectra clearly reveal the influence of the $TiO_2$ layer and charge transportation in the LS-NS devices. As further experimental evidence, we studied the influence of the $TiO_2$ layer and tracked changes in the TRF decay of the structures with a monolayer of CdTe NCs based on different polyelectrolyte polymer thicknesses. Subsequently, we attribute the shortening of lifetimes to the presence of charge transfer from the NC monolayer to the $TiO_2$ layer, which is energetically favorable. We believe that these results open the potential for the development of high-performance semi-transparent thin-film-based, large-area, and UV/visible sensing platforms.

## METHODS

**Synthesis of CdTe NCs.** First, we dissolved 4.59 g of $Cd(ClO_4)_2 \cdot 6H_2O$ in 500 mL of Milli-Q water, and then we added 1.33 g of TGA and adjusted the pH to 11.8−12.0. Then, we conducted $H_2Te$ gas flow by reacting 0.8 g of $Al_2Te_3$ with $H_2SO_4$ in the environment of a slow Ar flow. At 100 °C, the nucleation and growth of the NCs were initiated.

**Device Fabrication.** We washed an ITO film (80 nm) coated on a glass substrate by using ultrasonication in a mixture of 2 mL of Hellmanex in 100 mL of Milli-Q water for 20 min, followed by the baths in water, acetone, and isopropanol for 20 min each. We then continued our fabrication by depositing a 50 nm thick $HfO_2$ film, followed by a 10 nm thick $TiO_2$ layer using ALD (Savannah). Subsequently, we used a layer-by-layer self-assembly method with a computerized dip-coating system to deposit the NCs. Lastly, we laid a very thin (15 nm) transparent Al contact layer immediately on top of the CdTe NC monolayer via thermal evaporation.

**Device Characterizations.** We carried out all optoelectronic characterizations at room temperature and applied no external bias across the device. We measured the photovoltage buildup vs time characteristics using an Agilent Technologies parameter analyzer and a xenon light source with a monochromator. During the operation of the devices, each was connected to a 200 MΩ shunt resistor with the ITO contact grounded. We measured the optical power on the device using a Newport 1835C multifunction optical power meter. Because of the slight absorption of the $TiO_2$ layer, all devices were illuminated from the top (Al) side.

**Time-Resolved Fluorescence Measurements.** The decay curves were fitted with 3-exponentials ($\chi$2−1), which led to the best $\chi^2$ values, and the excited-state lifetimes for the samples were calculated via amplitude-averaging. The decay curves were also analyzed by 1/e fitting, and it was observed that there is a big consistency between the lifetimes obtained from both analysis techniques.

## ASSOCIATED CONTENT

### Supporting Information

Absorption spectrum of 10 nm $TiO_2$ grown by atomic layer deposition on $HfO_2$-coated glass substrate (Figure S1); absorption spectra of CdTe NCs (in solution) with the diameter size of (a) 2.9 nm and (b) 3.7 nm (Figure S2); photoluminescence excitation spectra (normalized) and absorption spectra (normalized) of the monolayer of CdTe NCs (in-film) with the diameter of 3.7 nm (Figure S3); variations of the photovoltage buildup based on 2.9 nm diameter CdTe NCs size at different excitation wavelengths without $TiO_2$ and with $TiO_2$ (Figure S4); photoluminescence and UV−vis-NIR absorption spectra of as-synthesized CdTe NCs (3.7 nm diameter) in solution at room temperature (Figure S5); and photoluminescence of a monolayer of CdTe NCs (3.7 nm diameter) at room temperature (Figure S6). This material is available free of charge via the Internet at http://pubs.acs.org.

## AUTHOR INFORMATION

### Corresponding Author

*E-mail: volkan@stanfordalumni.org.

### Notes

The authors declare no competing financial interest.

## ACKNOWLEDGMENTS

We acknowledge financial support, in part, by ESF EURYI, EU FP7 Nanophotonics4Energy NoE and TUBITAK under Project Nos. EEEAG 110E217, 111E189, and 112E183, and, in part, by NRF-CRP6-2010-02 and NRF RF 2009-09. H.V.D. gratefully acknowledges additional support from TUBA.

## ABBREVIATIONS

NC, Nanocrystal
LS-NS, Light-Sensitive nanocrystal skin
Al, Aluminum
$HfO_2$, Hafnium dioxide
ALD, Atomic layer deposition
ITO, Indium tin oxide
PDDA, Polydiallyldimethylammonium chloride
PSS, Polysodium 4-styrenesulfonate
TGA, Thioglycolic acid
PLE, Photoluminescence excitation
TRF, Time-resolved fluorescence

## REFERENCES

(1) Gaponenko, S. V. *Optical Properties of Semiconductor Nanocrystals*; Cambridge University Press: Cambridge, U.K., 1998.
(2) Kudera, S.; Carbone, L.; Manna, L.; Parak, J. W. *Semiconductor Nanocrystal Quantum Dots Synthesis, Assembly, Spectroscopy and Applications*; Rogach, A. L., Ed.; Springer: New York, 2008; pp 1−34.
(3) Talapin, D. V.; Rogach, A. L.; Kornowski, A.; Haase, M.; Weller, H. Highly Luminescent Monodisperse CdSe and CdSe/ZnS Nanocrystals Synthesized in a Hexadecylamine−Trioctylphosphine Oxide−Trioctylphospine Mixture. *Nano Lett.* **2001**, *1*, 207−211.
(4) Nozik, A. J. Nanoscience and Nanostructures for Photovoltaics and Solar Fuels. *Nano Lett.* **2010**, *10*, 2735−2741.
(5) Tang, J.; Kemp, K. W.; Hoogland, S.; Jeong, K. S.; Liu, H.; Levina, L.; Furukawa, M.; Wang, X.; Debnath, R.; Cha, D.; Chou, K. W.; Fischer, A.; Amassian, A.; Asbury, J. B.; Sargent, E. H. Colloidal-Quantum-Dot Photovoltaics Using Atomic-Ligand Passivation. *Nat. Mater.* **2011**, *10*, 765−771.
(6) Jean, J.; Chang, S.; Brown, P. R.; Cheng, J. J.; Rekemeyer, P. H.; Bawendi, M. G.; Gradečak, S.; Bulović, V. ZnO Nanowire Arrays for Enhanced Photocurrent in PbS Quantum Dot Solar Cells. *Adv. Mater.* **2013**, *25*, 2790−2796.
(7) Erdem, T.; Demir, H. V. Semiconductor Nanocrystals as Rare-Earth Alternatives. *Nat. Photonics* **2011**, *5*, 639798.
(8) Biteen, J. S.; Sweatlock, L. A.; Mertens, H.; Lewis, N. S.; Polman, A.; Atwater, H. A. Plasmon-Enhanced Photoluminescence of Silicon Quantum Dots: Simulation and Experiment. *J. Phys. Chem. C* **2007**, *111*, 13372−13377.
(9) Anikeeva, P. O.; Halpert, J. E.; Bawendi, M. G.; Bulovic, V. Quantum Dot Light-Emitting Devices with Electroluminescence Tunable over the Entire Visible Spectrum. *Nano Lett.* **2009**, *9*, 2532−2536.
(10) Oertel, D. C.; Bawendi, M. G.; Arango, A. C.; Bulović, V. Photodetectors Based on Treated CdSe Quantum-Dot Films. *Appl. Phys. Lett.* **2005**, *87*, 213505.

(11) Boberl, M.; Kovalenko, M. V.; Pillwein, G.; Brunthaler, G.; Heiss, W. Quantum Dot Nanocolumn Photodetectors for Light Detection in the Infrared. *Appl. Phys. Lett.* **2008**, *92*, 261113.
(12) Seker, U. O. S.; Mutlugun, E.; Martinez, P. L. H.; Sharma, V. K.; Lesnyak, V.; Gaponik, N.; Eychmüller, A.; Demir, H. V. Bio-Nanohybrids of Quantum Dots and Photoproteins Facilitating Strong Nonradiative Energy Transfer. *Nanoscale* **2013**, *5*, 7034.
(13) Lu, H.; Schops, O.; Woggon, U.; Niemeyer, C. M. Self-Assembled Donor Comprising Quantum Dots and Fluorescent Proteins for Long-Range Fluorescence Resonance Energy Transfer. *J. Am. Chem. Soc.* **2008**, *130*, 4815−4827.
(14) Murray, C. B.; Noms, D. J.; Bawendi, M. G. Synthesis and Characterization of Nearly Monodisperse CdE (E = S, Se, Te) Semiconductor Nanocrystallites. *J. Am. Chem. Soc.* **1993**, *115*, 8706−8715.
(15) Coe-sullivan, S. Quantum Dot Developments. *Nat. Photonics* **2009**, *3*, 315−316.
(16) Clifford, J. P.; Konstantatos, G.; Johnston, K. W.; Hoogland, S.; Levina, L.; Sargent, E. H. Fast, Sensitive and Spectrally Tuneable Colloidal-Quantum-Dot Photodetectors. *Nat. Nanotechnol.* **2009**, *4*, 40−44.
(17) Pelayo Garciía de Arquer, F.; Beck, F. J.; Bernechea, M.; Konstantatos, G. Plasmonic Light Trapping Leads to Responsivity Increase in Colloidal Quantum Dot Photodetectors. *Appl. Phys. Lett.* **2012**, *100*, 043101.
(18) Konstantatos, G.; Sargent, E. H. Nanostructured Materials for Photon Detection. *Nat. Nanotechnol.* **2010**, *5*, 391−400.
(19) Akhavan, S.; Guzelturk, B.; Sharma, V. K.; Demir, H. V. Large-Area Semi-Transparent Light-Sensitive Nanocrystal Skins. *Opt. Express* **2012**, *20*, 25255.
(20) Jasieniak, J.; Califano, M.; Watkins, S. E. Size-Dependent Valence and Conduction Band-Edge Energies of Semiconductor Nanocrystals. *ACS Nano* **2011**, *5*, 5888−5902.
(21) Jin, S.; Martinson, A. B. F.; Wiederrecht, G. P. Reduced Heterogeneity of Electron Transfer into Polycrystalline $TiO_2$ Films: Site Specific Kinetics Revealed by Single-Particle Spectroscopy. *J. Phys. Chem. C* **2012**, *116*, 3097−3104.
(22) Likovich, E. M.; Jaramillo, R.; Russell, K. J.; Ramanathan, S.; Narayanamurti, V. High-Current-Density Monolayer CdSe/ZnS Quantum Dot Light-Emitting Devices with Oxide Electrodes. *Adv. Mater.* **2011**, *23*, 4521−4525.
(23) Rogach, A. L.; Franzl, T.; Klar, T. A.; Feldmann, J.; Gaponik, N.; Lesnyak, V.; Shavel, A.; Eychmüller, A.; Rakovich, Y. P.; Donegan, J. F. Aqueous Synthesis of Thiol-Capped CdTe Nanocrystals: State-of-the-Art. *J. Phys. Chem. C* **2007**, *111*, 14628−14637.
(24) Reiss, P.; Protière, M.; Li, L. Core/Shell Semiconductor Nanocrystals. *Small* **2009**, *5*, 154−168.
(25) Akhavan, S.; Cihan, A. F.; Bozok, B.; Demir, H. V. Nanocrystal Skins with Exciton Funneling for Photosensing. *Small* **2014**, DOI: 10.1002/smll.201303808.
(26) Mamedov, A. A.; Belov, A.; Giersig, M.; Mamedova, N. N.; Kotov, N. A. Nanorainbows: Graded Semiconductor Films from Quantum Dots. *J. Am. Chem. Soc.* **2001**, *123*, 7738−7739.
(27) Sukhovatkin, V.; Hinds, S.; Brzozowski, L.; Sargent, E. H. Colloidal Quantum-Dot Photodetectors Exploiting Multiexciton Generation. *Science* **2009**, *324*, 1542−1544.
(28) Ostrander, J. W.; Mamedov, A. A.; Kotov, N. A. Two Modes of Linear Layer-by-Layer Growth of Nanoparticle-Polylectrolyte Multilayers and Different Interactions in the Layer-by-Layer Deposition. *J. Am. Chem. Soc.* **2001**, *123*, 1101−1110.
(29) Shavel, A.; Gaponik, N.; Eychmüller, A. Efficient UV-Blue Photoluminescing Thiol-Stabilized Water-Soluble Alloyed ZnSe(S) Nanocrystals. *J. Phys. Chem. B* **2004**, *108*, 5905−5908.
(30) Komarala, V. K.; Rakovich, Y. P.; Bradley, A. L.; Byrne, S. J.; Corr, S. A.; Gun'ko, Y. K. Emission Properties of Colloidal Quantum Dots on Polyelectrolyte Multilayers. *Nanotechnology* **2006**, *17*, 4117−4122.
(31) Akhavan, S.; Gungor, K.; Mutlugun, E.; Demir, H. V. Plasmonic Light-Sensitive Skins of Nanocrystal Monolayers. *Nanotechnology* **2013**, *24*, 155201.
(32) Valeur, B. *Molecular Fluorescence: Principles and Applications*; WILEY-VCH: Weinheim, 2002.
(33) Lakowicz, J. R. *Principles of Fluorescence Spectroscopy*; Springer: New York, 2006.
(34) Förster, T. Zwischenmolekulare Energiewanderung Und Fluoreszenz. *Annu. Phys.* **1948**, *437*, 55−75.
(35) Yeltik, A.; Kucukayan-Dogu, G.; Guzelturk, B.; Fardindoost, S.; Kelestemur, Y.; Demir, H. V. Evidence for Nonradiative Energy Transfer in Graphene Oxide Based Hybrid Structures. *J. Phys. Chem. C* **2013**, *117*, 25298−25304.